WELDING-INDUCED BUCKLING INSTABILITIES IN THIN PLATES

Han, Myoung-Soo [1]* and Tsai, Chon-Liang [2]

[1] Test & Evaluation R&D Team, Daewoo Shipbuilding & Marine Engineering Co., Ltd.,
1 Ajoo-dong, Koje-si, KyoungNam, Korea, 656-714, mshan@dsme.co.kr
[2] Department of Industrial, Welding and System Engineering, The Ohio State University,
1248 Arthur E. Adams Drive, Columbus, Ohio 43221, USA, tsai.1@osu.edu

ABSTRACT

Welding-induced buckling distortion is one of the most problematic concerns in both design and fabrication of welded thin-plate structures. This paper deals with experimental and numerical results of the welding-induced longitudinal and/or buckling distortion occurring in welding of 6mm-thick AH36 high strength steel plates. Effects of the heat input and the plate size on the distortion were experimentally evaluated for square plates. Bead-on-plate welding was performed with the submerged arc welding process along the middle line of plate specimens. Experimental results showed that the longitudinal distortion made a single curvature in the plate, and the distortion magnitude along the weld centerline was proportional to the heat input and the plate size. The experimental results were used to examine the validity of the numerical simulation procedure for welding-induced distortion where the longitudinal distortion mode and magnitude were numerically quantified. Three-dimensional, large deformation, welding simulations were performed for selected weld models. Numerical results of the distortion mode and magnitude were in a good agreement with experimental ones. Depending on the presence of halting the distortion growth during the cooling cycle of welding, the condition discriminating buckling distortion from longitudinal distortion was established. Eigenvalue analyses were performed to check the buckling instability of tested plates with different sizes subjected to different heat inputs. The perturbation load pattern for the analysis was extracted from longitudinal inherent strain distributions. Critical buckling curve from the eigenvalue analyses revealed that the buckling instability is manifested when plate size or heat input increases.

KEYWORDS

Welding-induced Buckling Distortion, Eigenvalue Analysis, Inherent Strains, Nil-plasticity Peak Temperature, Finite Element Analysis (FEA)

1. Introduction

Welding of thin plates can cause extensive buckling distortion that results in undesirable conditions including insufficient structural integrity and manufacturing unreliability. It is difficult to obtain closed forms of analytical buckling solutions for plates under welding thermal cycles since temperature histories during welding introduce non-uniform transient stress fields. Remarkable developments in computer technology in recent years have improved the numerical prediction capability for welding distortion. Compared to extensive study on other types of welding deformations, however, the buckling distortion has not been much investigated since buckling

characterization in local detail of the welded area as well as the large spatial structural domain would require extensive computation time, and substantially limit available resources.

It is generally accepted that welding distortion is caused by incompatible inherent strains accumulated during welding. Upon cooling, tensile stresses are built up in the inherent strain region while compressive stress fields are produced away from it. Those compressive stress fields as a whole act as membrane forces that cause the plate to buckle, and the inherent strains play a decisive role in the buckling process. Therefore, it is surmised that a rational predictive methodology for the buckling instability can be found if one can approximate the strains distributed in and around the weld region.

In this study, a fundamental study on the prediction and control of welding-induced buckling distortion in thin plates was conducted through correlating inherent strains with welding process variables and the degree of constraints. The approximated inherent strain fields were utilized for the buckling prediction performed by the eigenvalue analysis. Evolutional characteristics of welding-induced buckling distortion were observed from the three-dimensional welding simulation. Experimental studies were also performed to verify the numerical prediction capability of welding-induced buckling distortion.

2. Procedures

2.1. Experimental procedures

All the specimens made of 6mm-thick AH36 steel plates were square shape. Details of specimen dimension and welding conditions are given in Table 1. Specimens of 500mm in length×500mm in width (5A through 5G in Table 1) were used to evaluate the effect of the heat input ranging from 558 J/mm to 1280 J/mm. In order to observe the dimensional sensitivity of the distortion, experiments under the constant heat input of 1097 J/mm were also performed on the specimens with different sizes (3E through 10E in Table 1). The submerged arc welding process with consumables in accordance with AWS A5.17 (F7A4-EL8) was used to make the bead-on-plate welds along the middle line of the specimen. End tabs of 120mm×160mm were attached to both ends of specimens to create continuous beads across the edge regions. The electrode extension of 25mm and the dc (+) electrode polarity (DCEP) were used in all the welding procedures. All the experiments were carried out at ambient temperature (25.8°C) and under constraint-free boundary conditions in thermal and structural aspects.

Table 1 Specimen dimension and welding variables applied

Weld model	Plate size (mm)		Welding variables				
	Length	Width	Wire diameter (mm)	Current (Amperes)	Voltage (Volts)	Speed (mm/min)	Heat input (J/mm)
5A	500	500	2.0	300	31	1000	558
5B	500	500	2.0	300	31	750	744
5C	500	500	2.0	300	31	650	859
5D	500	500	2.0	300	31	550	1015
5E	500	500	3.2	400	32	700	1097
5F	500	500	3.2	400	32	650	1182
5G	500	500	3.2	400	32	600	1280
3E	300	300	3.2	400	32	700	1097
4E	400	400	3.2	400	32	700	1097
10E	1000	1000	3.2	400	32	700	1097

Before welding, grids with intervals of 50mm were made on the back surface of specimens to measure the flatness at intersection points of the grids. The measurements were made both before and after welding, thus calculating the normal displacement due to welding from the difference between the two measurements.

2.2. Numerical procedures

Two- and three-dimensional finite element analyses, using the commercial package ABAQUS, were carried out to numerically investigate the welding-induced longitudinal distortion in plates. A decoupled thermo-elastic-plastic behavior of materials was assumed for the numerical welding simulation. Two-dimensional welding simulations were performed on the cross-section model of the specimen in order to standardize the longitudinal inherent strain fields dependent upon welding conditions and plate sizes and therethrough to utilize the two-dimensionally determined strain fields for the three-dimensional buckling prediction performed through the eigenvalue analyses. The three-dimensional welding simulation was also carried out. In order to enhance the simulation accuracy for nonlinear geometrical behaviors, the large deformation theory was incorporated into the thermo-elastic-plastic finite element analysis. Those procedure and method for the numerical welding simulation are illustrated in the reference [1].

3. Results

3.1 Evolution of longitudinal distortion

Fig. 1 compares the effect of welding heat input on the vertical displacement (U_z) at the plate center from experiments and three-dimensional welding simulations. Reasonable agreement between the two can be found. The values of U_z at the plate center are strongly dependent upon heat input although a wavy shape against the trend exists in the experimental observation. In arc welding process, the higher heat input brings the wider peak temperature boundary, and hence it makes the larger plastic zone in and around the weld region. After cooling,

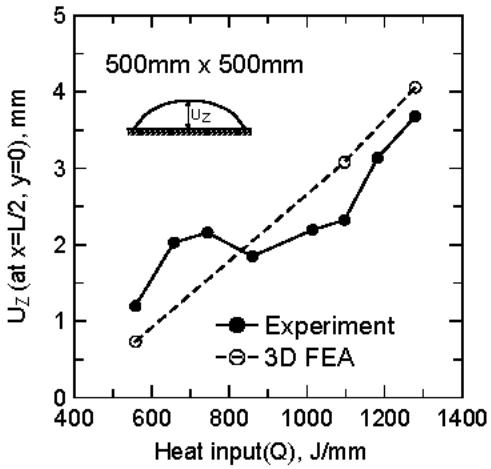

Fig. 1 Effect of heat input on δ_B

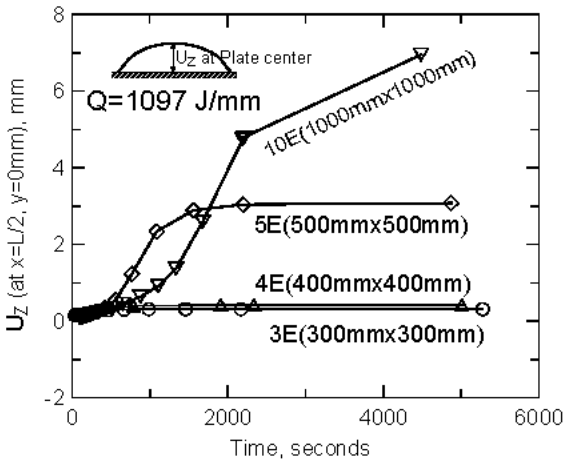

Fig. 2 Variation of δ_B in plates with different sizes

the tensile stress field is eventually formed within the plastically deformed region, and the compressive stress field is induced in the remaining area to satisfy the equilibrium. This implies that the wider tensile zone due to the higher heat input form the more compressive stress, which makes the plates more prone to buckle.

Fig. 2 illustrates the effect of plate size on the variation of the vertical displacement (U_z) at the plate center, representing the evolution of the longitudinal distortion during welding cycles. The halt of the displacement growth can be observed except for the largest model (10E) where the growth of the vertical displacement continued to the completion of the welding cycles. Additionally, it is seen that the onset of the displacement growth in the smaller model is made at the earlier time of the cooling cycle, but the transient condition that causes the longitudinal distortion is quickly disappeared, halting the growth of the distortion.

Figs. 3 and 4 show the transient variation of the vertical displacement (U_z) and longitudinal stresses (σ_{xx}) on the top and bottom surfaces in the simulated models, 5E and 10E. Vertical displacements were taken from the node located at the center of simulated models, and stresses were those at the centroid of the outermost elements

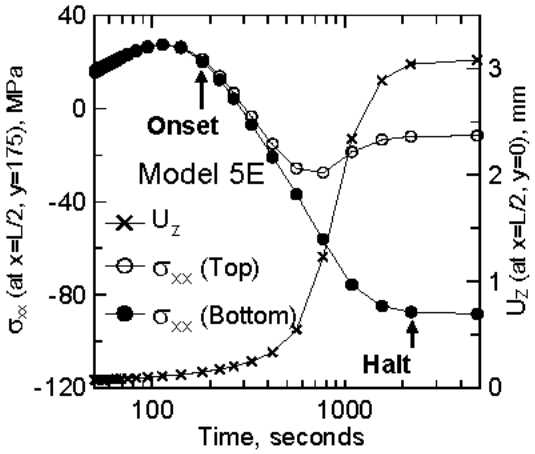

Fig. 3 Evolution of longitudinal distortion in 5E model.

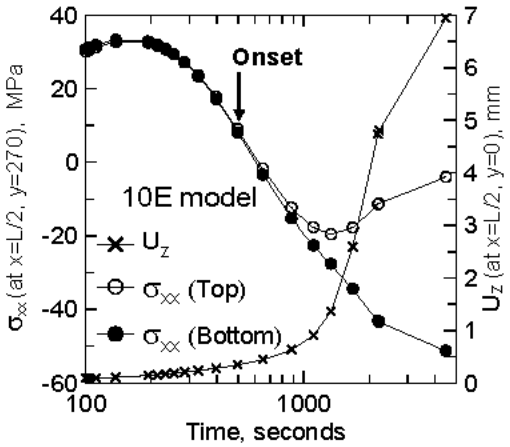

Fig. 4 Evolution of longitudinal distortion in 10E model.

toward the top and bottom surfaces 175mm (for 5E model) and 270mm (for 10E model) away from the weld centerline at the mid-length section. These two figures represent the evolutional variation of the longitudinal stress and distortion occurring in the small and large plates. Stress variations in both plates reveal that stress deviations between the top and bottom surfaces take place at an early stage during the cooling cycle. In the large plate (10E), the stress deviation continues to grow from the onset to the completion of welding cycles, which can be also demonstrated by the corresponding increase of the vertical displacement. On the other hand, the stress deviation in the small plate (5E) occurs for a limited cooling period, whereafter both the vertical displacement and the stress deviation in Fig. 3 become constant. Stress deviations, shown in Figs. 3 and 4, are closely related to the growth of the longitudinal distortion represented by the vertical displacement since the longitudinal distortion creates the bending stress through the plate thickness that is the cause of the stress deviation, and the deviation increases with the increase of the distortion. When the growth of the vertical displacement is hindered, the stress deviation will correspondingly retarded.

As shown in Fig. 2, the evolution of the longitudinal distortion in small plates clearly differs from that in larger plates since it occurred for a limited period of the cooling cycle while non-linear thermal strain fields substantially prevailed. On the other hand, the vertical displacement and stress deviation in the largest plate studied (Fig. 4) continued to grow until the completion of the cooling cycle. The distortion in this plate appears

to be the buckling distortion since any longitudinal distortion other than buckling may not explain such a high growth of the vertical displacement that continued until the completion of the cooling cycles. In order to assure the occurrence of buckling in the weld model 10E, the welded plate should be instable when stability analyses are performed on the plate under the residual stress state.

3.2 Prediction of welding-induced buckling instability

Eigenvalue analyses are introduced to estimate the critical condition for the buckling instability of welded plates. The perturbation load patterns for eigenvalue analyses are based on longitudinal inherent strains computed by two-dimensional welding simulations for the cross-section model of welds.

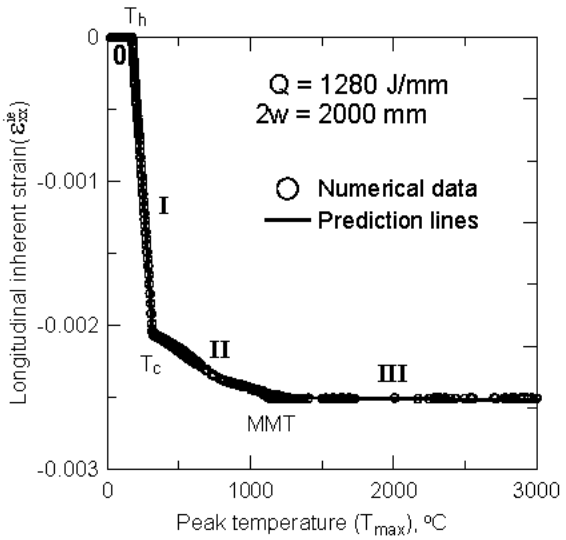

Fig. 5 Relationship between peak temperatures and longitudinal inherent strains

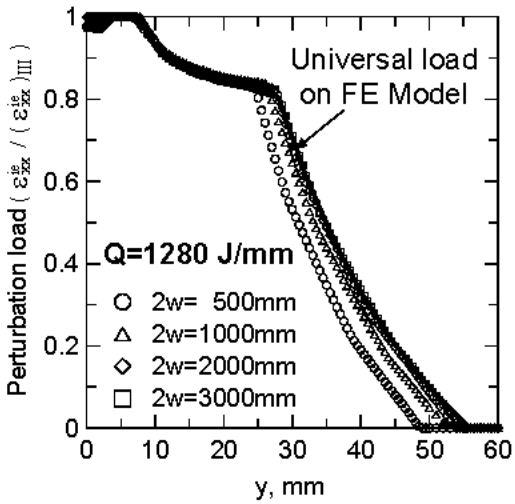

Fig. 6 Normalized inherent strains and perturbation load pattern for eigenvalue analyses

Fig. 5 illustrates the relationship between peak temperatures and longitudinal inherent strains obtained from a weld model subjected to the heat input of 1280 J/mm. The inherent strain field, related to the peak temperature field, is distinctively divided into four zones. Inherent strains are not produced in the zone (ZONE 0) where peak temperatures are less than a threshold value named as the nil-plasticity peak temperature (T_h in Fig. 5) which was used in this study as a prime parameter for characterizing inherent strain fields. Once T_h is given by the numerical welding simulation, other boundary temperatures between adjacent zones can easily be determined. MMT in Fig. 5, abbreviating the mechanical melting temperature [2], is given by high temperature material properties. Considering the temperature range that causes plastic strains during the cooling cycles, the relationship between T_h and T_c approximately turns out to be $T_c = 2 \cdot T_h - T_0$ where T_0=ambient temperature. Solid lines in Fig. 5 were drawn by prediction formulas developed in this study [1]. The peak temperatures and T_h were used as parameters for the prediction. Agreement between simulated and predicted results is apparent.

In order to derive the perturbation load pattern, all inherent strain values were normalized by the constant strain for ZONE III in Fig. 5, $\left(\varepsilon_{xx}^{ie}\right)_{III}$, to calculate the fraction varying from 0 to 1. Fig. 6 shows the normalized inherent strain distributions for weld models with different plate sizes where the heat input of 1280 J/mm is

equally applied. The distribution in the figure gradually converges when the plate size increases. In this study, the data giving the widest distribution (the solid line in Fig. 6) is selected as the universal perturbation load pattern for weld models subjected to the same heat input.

Once the perturbation load pattern is determined, the execution of eigenvalue analyses is straightforward. The load pattern from Fig.6 is directly given to the finite element model as temperatures varying between 0 and 1 to produce the thermal strain distribution. A negative thermal expansion coefficient, α_{eigen}, is arbitrary defined for this purpose. Because the peak temperature in the welding direction is uniform in analyzing the plate continuously welded, the same load pattern was applied to meshes along the welding direction. Applying the universal perturbation load pattern, corresponding to heat input, to the plate model, the eigenvalue analysis calculates the lowest positive eigenvalue, λ_c , and the corresponding eigenvector, $\{dD\}_c$, for a given combination of plate size and heat input. The buckling strain for ZONE III, ε_B, which is needed to buckle the plate for a given combination of size and heat input, can then be determined by

$$\varepsilon_B = \alpha_{eigen} \cdot \lambda_c \tag{1}$$

For each heat input level, the critical value of the plate size (or width) exists when

$$|\varepsilon_B| = \left|\left(\varepsilon_{xx}^{ie}\right)_{III}\right| \tag{2}$$

Thus, the plate of which width is larger than the critical value given by Eq. (2) will be instable to buckling under the given heat input level.

In Fig. 7, the relationship between the critical width and critical heat input is drawn to provide the critical curve that characterizes buckling distortion in welded plates. If the combination of plate size and heat input

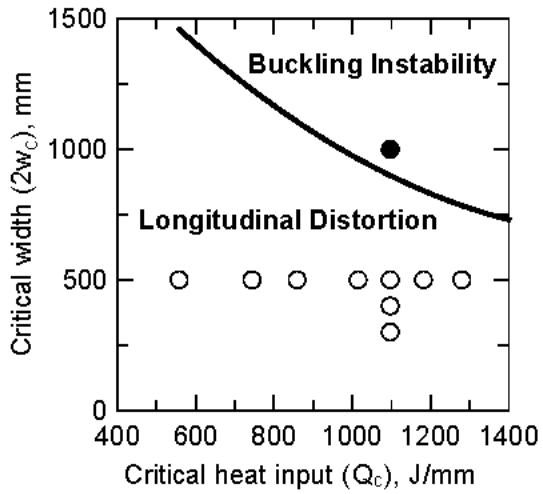

Fig. 7 Critical curve for welding-induced buckling instability.

exists in the right side of the curve, it is possible for buckling instability to occur. The buckling instability is to be manifested as either plate size or heat input or both increases. Data points in Fig. 7 display the combination of plate size and heat input considered in experiments discussed in the previous section. The solid circles correspond to the case where the longitudinal distortion continued to grow until the completion of the cooling cycle (10E model), and it exists within the regime of the buckling instability predicted by the eigenvalue analysis.

Therefore, the longitudinal distortion extended to the completion of the cooling cycle in the three-dimensional large deformation analysis is characterized as the buckling instability by the eigenvalue analysis. The open circles, on the other hand, correspond to the condition at which the longitudinal distortion in the large deformation analysis occurred during the limited period of the cooling cycle. Based on the eigenvalue prediction, those longitudinal distortions are not associated with the buckling instability. The critical curve shown in Fig. 7 characterizes the possibility of the buckling instability under the residual stress state. Therefore, the curve may not characterize those limited longitudinal distortions as the buckling instability since the longitudinal distortions stops before the residual state is established in the welded plate.

4. Summary

In this study, experiments and numerical analyses were performed on square-shaped thin plates in order to investigate the welding-induced longitudinal distortion. In experiments, bead-on-plate welding onto 6mm-thick AH36 steel plates was performed with the submerged arc welding process. Effects of welding heat input and plate sizes on the welding distortion were examined. Three-dimensional, thermo-elastic-plastic, large deformation analyses were performed to numerically simulate the welding distortion. In addition, a predictive methodology for welding-induced buckling distortion was presented. Eigenvalue analysis was exploited to characterize the buckling instability. In order to extract the perturbation load pattern for the eigenvalue analyses, a fundamental study on longitudinal inherent strain distributions were performed on two-dimensional cross section models of different sizes and subjected to different heat inputs. Significant findings observed through the study are summarized as follows:

1) The peak temperatures and the nil-plasticity peak temperature uniquely determined the fields and the magnitudes of longitudinal incompatible strains.
2) The critical curve obtained from eigenvalue analyses utilizing incompatible strains showed that the buckling instability is manifested as plate size or heat input increases.
3) The onset of longitudinal welding distortion was strongly influenced by transient temperature fields. The more intensified thermal field was required for the onset in the smaller plate subjected to the smaller heat input. Longitudinal distortion in small plates grew for a limited period of the cooling cycle while it continued to grow in large plates until the completion of the cooling cycle.
4) Buckling instability predicted by eigenvalue analyses was closely related to the longitudinal distortion continued to grow until the completion of the cooling cycle.

References

[1] M. S. Han: Ph.D. Dissertation, The Ohio State University, Ohio, USA, March (2002).

[2] Y. Ueda, M. G. Yuan: Transactions of the ASME, Journal of Engineering Materials and Technology, 115(1993), October, p. 417